22

Sunram 5: A Magnetic Resonance-Safe Robotic System for Breast Biopsy, Driven by Pneumatic Stepper Motors

Vincent Groenhuis[1], Françoise J. Siepel[1] and Stefano Stramigioli[1,2]

[1]*Robotics and Mechatronics, University of Twente, Enschede, The Netherlands*
[2]*ITMO University, Saint Petersburg, Russia*

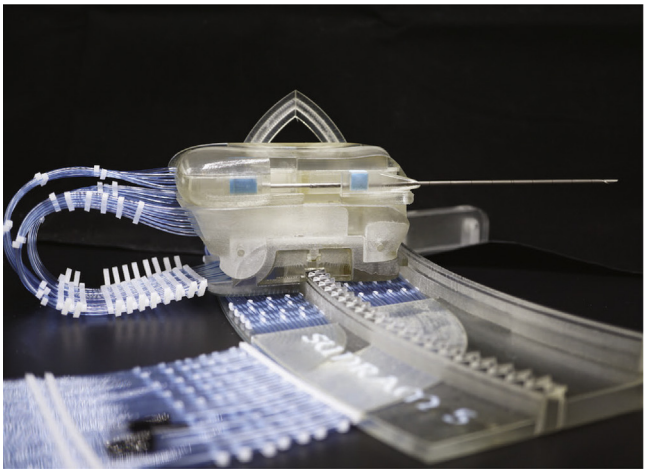

CHAPTER FOCUS
ENGINEERING

TECHNOLOGY
ROBOTIC & IMAGE-GUIDED

LINK TO VIDEO

ABSTRACT

Sunram 5 is the fifth-generation magnetic resonance (MR)-safe robotic system for breast biopsy. It has five degrees of freedom and is driven by six linear and curved pneumatic stepper motors plus three singular cylinders, all constructed by rapid prototyping techniques. The design, production, and evaluation of both single pneumatic cylinders and various type of stepper motors are described in detail in this chapter. Control strategies are also discussed such as how multiple motors can work together in order to achieve both high speed and high accuracy, despite the relatively low stepping frequencies associated with long pneumatic lines between controller and motor. Sunram 5 also includes a breast fixation system, an emergency needle ejection mechanism, and fast and precise needle insertions under near-realtime MR imaging (MRI) guidance, giving potential to improve accuracy and efficiency in MRI-guided breast biopsy procedures.

Handbook of Robotic and Image-Guided Surgery. DOI: https://doi.org/10.1016/B978-0-12-814245-5.00022-0

22.1 Introduction

22.1.1 Clinical challenge

Breast cancer is the most commonly diagnosed cancer type among women [1]. Early detection is essential for a good prognosis. In many countries breast cancer screening programs have been set up. Mammography (X-ray) is the primary imaging modality, as it is quick and able to detect the majority of cancers. In addition, ultrasound (US), palpation, computed tomography, and/or magnetic resonance (MR) imaging (MRI) may be used for more conclusive screening.

MRI has the highest sensitivity of all imaging modalities. It makes a 3D scan with (sub-)millimeter resolution with good contrast between different types of tissue. After inserting a contrast agent, areas of angiogenesis (local growth of veins) can be distinguished.

Certain patient groups may undergo MRI screening even if no abnormalities are found on mammography or US. Women carrying the *BRCA 1* or *2* gene have an elevated risk for developing breast cancer and benefit from periodic MRI screening [2]. Additionally, women with inexplicable complaints in the breast (e.g., pain) may be advised to undergo MRI screening. Finally, MRI scans may also be useful for the surgeon to prepare for breast surgeries.

When a suspicious lesion is found, a biopsy is required for accurate histological evaluation. This is first attempted under US guidance, which is a relatively easy procedure if the lesion is well visible on US. In this procedure the radiologist inserts a biopsy needle into the breast toward the lesion. When correctly positioned, the biopsy gun is fired, capturing a tissue sample of the suspicious lesion which is subsequently stored for pathology assessment. This method is the gold standard in determining the malignancy of suspicious lesions.

In some cases the lesion is not visible on US, but only on MRI. An MR-guided biopsy is then necessary. In this procedure the radiologist inserts a biopsy needle using a grid or postpillar system. This is normally performed outside the MRI scanner due to accessibility constraints of the scanner bore. The patient has to be moved in and out of the scanner multiple times in the procedure. Small movements of the breast due to respiration and tension may cause displacement of the lesion to be sampled, making it difficult to precisely target it. Also, the spacing of the grid introduces a discretization error when this method is used. To compensate for these errors, a relatively large needle (9 ga, equivalent to 3.8 mm) is generally used, and multiple tissue samples are acquired to obtain a high confidence of acquiring at least one tissue sample of the lesion. One example system is the vacuum-assisted breast biopsy (VABB) system by Hologic. Still, the confirmation scan may indicate an inadequate needle placement, requiring repositioning of the needle, leading to additional tissue damage or a false-negative biopsy.

In order to resolve the shortcomings of the manual MRI-guided breast biopsy procedure, the needle should not be inserted blindly outside the MRI scanner, but inside the scanner bore itself. This more or less implies the necessity of a robotic system to position, align, and insert the biopsy needle due to accessibility constraints. This eliminates the possibility of patient movements and allows for (near-)realtime imaging guidance during robotic needle insertion. Additionally, robotic systems potentially allow for more precise needle insertions. With such a system, a relatively thin (16 ga, equivalent to 2.1 mm) biopsy needle is sufficient, resulting in considerably less tissue damage compared to conventional systems such as the VABB.

22.1.2 Magnetic resonance imaging compatibility of surgical robots

An important requirement for devices inside the MRI scanner is that these are safe to use in the specific environment. The ASTM F2503 standard defines three categories of MRI devices: MR safe, MR conditional, and MR unsafe [3]. The MR-safe requirement implies that the device is free of metallic, ferromagnetic, and conductive materials and therefore is inherently safe to use in all MRI scanners. This is regardless of the field strength and other parameters such as maximum gradients and minimum distance to patient. The MR conditional classification indicates that the device is only safe when certain given conditions are all met, while devices with the MR-unsafe classification pose unacceptable risks and cannot be used in any MRI environment. This scheme replaces the former one (MR compatible/safe), which is known to cause confusion and errors: many "MRI-compatible" devices were only tested under certain conditions and sometimes resulted in unsafe behavior in other environments, leading to serious risks.

22.1.3 Actuation methods for magnetic resonance-safe/conditional robots

The MR-safe/conditional requirement implies that conventional electromagnetic motors cannot be directly used in actuation of any MR robot. Several alternative actuation methods have been proposed and demonstrated:

- Piezo motors and ultrasonic motors are electric motors that only cause limited interference with the MRI's magnetic field. Using dedicated control electronics and taking certain precautions, such motors may be classified MR conditional and may be usable in actuation of MRI robots [4–6]. A drawback is that piezo/ultrasonic motors cannot be classified MR safe due to the use of electricity and metallic materials, so the MRI safety and imaging quality aspects have to be reevaluated each time that operating conditions are expanded.
- Bowden cables transport energy via solid wires guided through tubes [6,7]. Instead of tubes a system of pulleys can also be used. These techniques allow to place conventional motors away from the robot (outside the Faraday cage of the MRI scanner). If the wires and Bowden tubes (or pulleys) are made of nonmetallic materials, the system could be made MR safe. Friction, backlash, and elasticity in the rigid materials may make an effective energy transfer difficult, especially when many bends are present in the transmission line.
  - Pneumatics use clean air as an energy transfer medium which is abundant in hospitals and laboratory environments. As small leakages are acceptable, pneumatic cylinders can be manufactured using rapid prototyping techniques. Important limitations are the compressibility of the medium which makes precise position control of a single cylinder difficult [8,9], and also the long distance between the (MR-unsafe) controller manifold and robot leads to long pneumatic lines which result in relatively low bandwidth.
  - Hydraulics make use of liquid to deliver power to the robotic system [10,11]. The liquid is kept in a closed system with a compressor and valves and leaks are to be avoided. A hydraulic device requires the use of precisely engineered components, which makes rapid prototyping relatively difficult compared to other techniques.
  - Actuation by magnetic spheres driven by gradients of the MRI scanner have also been demonstrated [12]. This technique is relatively complicated as it requires precise control of the MRI's gradients while at the same time mitigating the imaging artifacts induced by the magnets.
  - Shaped memory alloy (SMA) actuators generate unidirectional movements when heat is applied to an SMA spring. The heat can be generated by applying current through the SMA spring, of which the self-resistance results in resistive heating. Bidirectional movement is generated using complementary pairs of SMA springs [13]. The use of metallic materials in the SMA actuators and the application of current through it make the SMA actuators MR conditional at best.

The authors of this chapter use pneumatics as the energy transfer method in the form of pneumatic stepper motors. We show that fast and precise control is possible, despite the low bandwidth and lack of direct position feedback.

22.1.4 State of the art

Many MRI surgical robots have been developed in the past by various research groups. In this chapter a selection of robotic systems driven by pneumatic stepper motors is discussed: first three robots by other research groups and then five robots by the authors of this chapter.

22.1.4.1 Pneumatic magnetic resonance imaging robots by Stoianovici, Bomers, and Sajima

Stoianovici et al. developed several MRI robots for prostate biopsy. One example is the MrBot, shown in Fig. 22.1A [14]. It is driven by six PneuStep rotational stepper motors of which a schematic cross-section is shown in Fig. 22.2A. The PneuStep motor consists of three diaphragm cylinders that are connected to an internal gear. By alternatingly pressurizing the three cylinders, the internal gear is translated along a circular trajectory and its hoop gear in turn engages a spur gear. A leadscrew mechanism then converts the rotational motion of the spur gear into linear motion, resulting in movement of the robotic system. PneuStep makes use of optical positional encoders to detect and correct for missing steps, allowing to operate it at higher stepping speeds when less than maximum torque is needed. The valve manifold is put inside a shielded enclosure within the MRI room, allowing to reduce the tube lengths to a minimum [16].

The Soterial Remote Controlled Manipulator by Bomers et al. is shown in Fig. 22.1B. Like MrBot, this robot is designed for prostate interventions [15]. It is driven by five pneumatic stepper motors of which a schematic drawing is shown in Fig. 22.2B. Its five cylinders have cone tips mounted on the pistons which engage on a two-dimensional (2D) pattern of holes on the rod. Pressurization of one cylinder pushes the associated cone tip into one hole, forcing the hole to align with the cone tip by the associated wedge mechanism and thereby introducing a displacement. Sequential pressurization of the right combination of cylinders results in either a screw movement or a linear movement of the rod, resulting in a small or large displacement of the robot linkages. The cylinders are double-acting; a single tube is used for the return stroke of all five pistons so that six tubes are used per actuator [17].

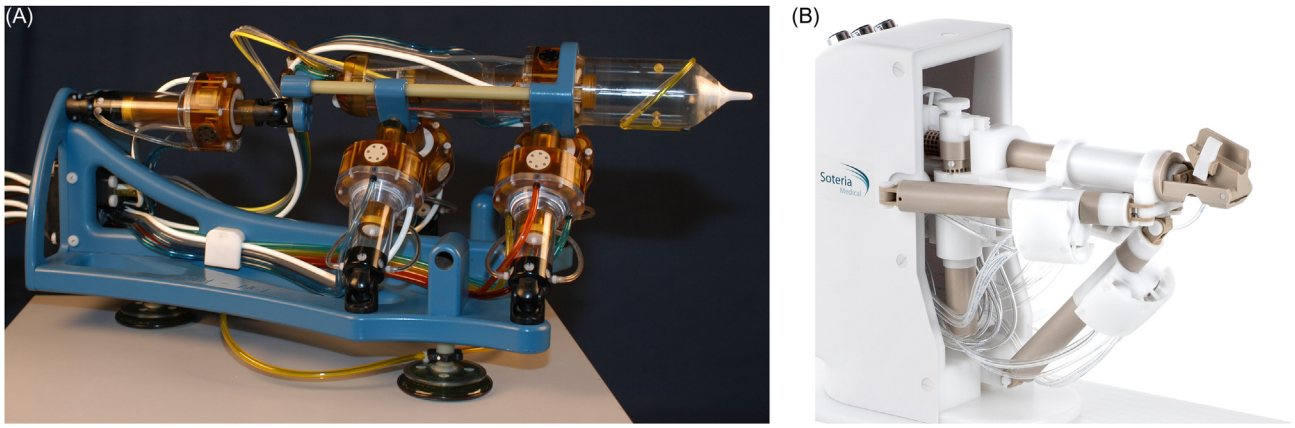

FIGURE 22.1 Two state-of-the-art MRI manipulators driven by pneumatic stepper motors. (A) MrBot by Stoianovici et al. [14]. (B) Soteria RCM by Bomers et al. [15]. *MRI*, Magnetic resonance imaging; *RCM*, remote controlled manipulator.

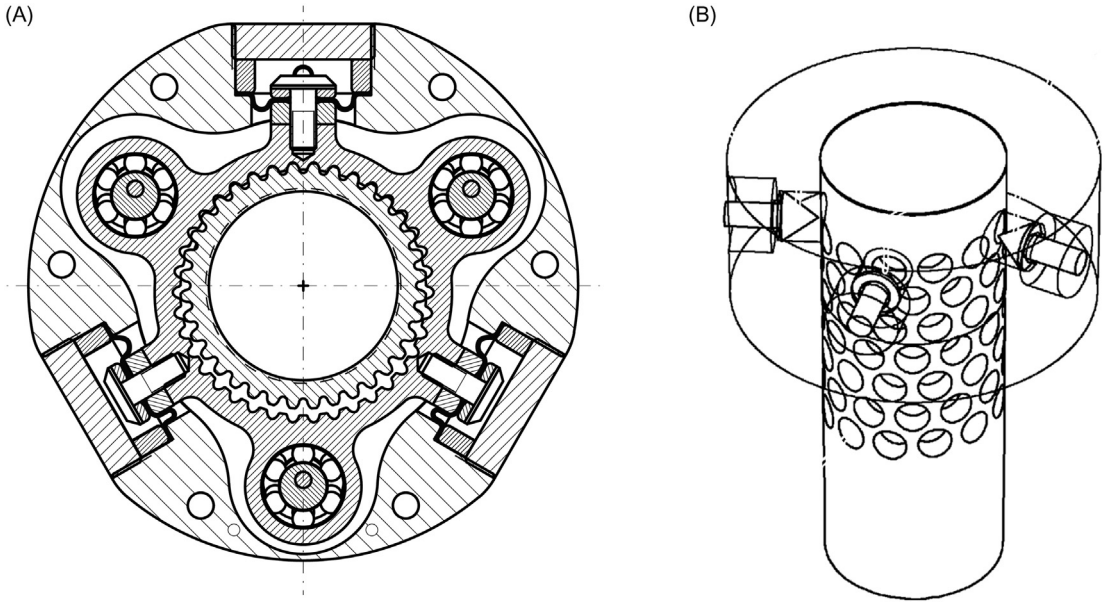

FIGURE 22.2 Pneumatic motors used to actuate the corresponding manipulators in Fig. 22.1. (A) PneuStep by Stoianovici et al. [16], (B) pneumatic stepper motor by Bosboom et al. [17].

Sajima et al. developed a manipulator driven by rotational stepper motors [18,19]. Each stepper motor consists of three single-acting cylinders that act on a rotation gear by means of a wedge mechanism. By sequentially pressurizing the three cylinders the gear is driven around in either direction. In this design the gears have to be back-drivable in order to allow retraction of the pistons in the nonpressurized cylinders for continuous movements. A leadscrew finally converts the rotational motion of the gear into linear motion of the manipulator linkages.

An important limitation of the design of Sajima is that the wedge mechanism must be back-drivable due to the use of single-acting cylinders. This implies that the teeth cannot have sharp angles and significant torque is lost by friction of the sliding surfaces. On the other hand, Sajima's design is relatively compact and easy to manufacture compared to the designs of Stoianovici and Bomers.

The low nominal stepping frequency resulting from the long pneumatic tubes is an issue which has to be addressed in order to achieve both high speed and high accuracy. Stoinanovici's design utilizes position encoders which allow to speed up the motors when less than maximum torque is needed, while Bomers' design uses a 2D hole pattern that enables both large and small actuation steps.

TABLE 22.1 Comparison of Stormram 1–4 and Sunram 5.

Robot	Dimensions (mm)	DoF	Workspace	Motor step size	Stepper motor force	Accuracy
Stormram 1	290 × 290 × 310	7	Small	1.3 mm	30 N@0.4 MPa	~2 mm (free air)
Stormram 2	140 × 140 × 140	5	~0.4 L	1 mm	15 N	~2 mm (free air) 4.7–7.3 mm (MRI)
Stormram 3	185 × 155 × 140	5	<2 L	0.67 mm	13/70 N, @0.3 MPa	~2 mm (free air)
Stormram 4	200 × 115 × 50 (full) 72 × 51 × 40 (moving)	4	2.2 L	0.25 mm	63 N @0.65 MPa	0.7 mm (free air) 1.3 mm (MRI)
Sunram 5	200 × 140 × 90 (full) 107 × 72 × 56 (moving)	5	Large	0.3 mm	>60 N	<1 mm (free air)

DoF, Degree of freedom; *MRI*, magnetic resonance imaging.

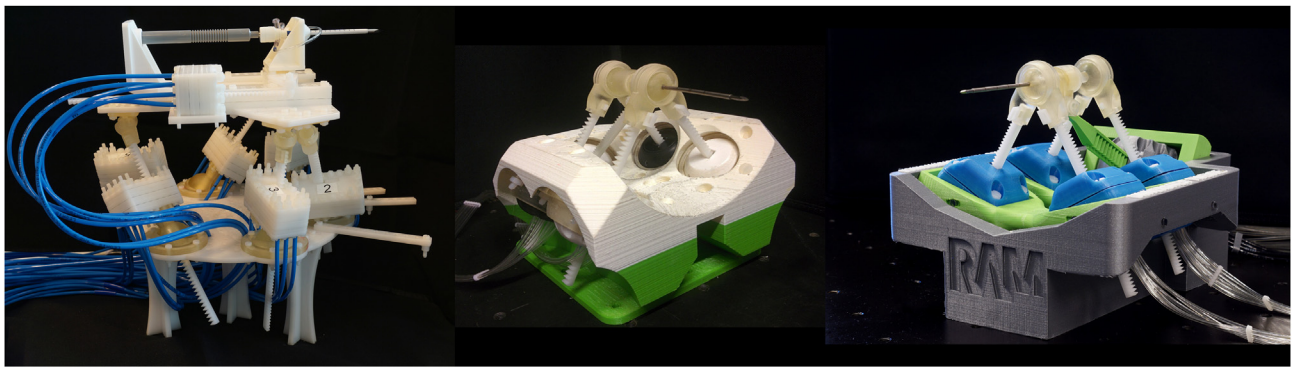

FIGURE 22.3 Stormram 1 (left), Stormram 2 (center), and Stormram 3 (right).

22.1.4.2 Stormram 1–4 and Sunram 5

Five MR-safe breast biopsy robots have been developed by the authors of this chapter. All of them are driven by pneumatic linear or curved stepper motors and rapid prototyped by 3D printing and laser-cutting techniques. Table 22.1 lists the main characteristics of each of the five generations.

Stormram 1 (Fig. 22.3, left) was developed in 2014 and has seven degrees of freedom (DoFs) [20]. Its large size and small workspace make it unsuitable for practical applications, so in 2015 the Stormram 2 was developed (Fig. 22.3, center) with five DoFs. This robot is driven by stepper motors integrated inside 45 mm ball joints for compactness [21]. In the following year Stormram 3 was developed (Fig. 22.3, right), also with five DoFs and with improved accuracy, force characteristics, and workspace thanks to redesigned joints and smaller step sizes [22]. Still, the use of a parallel kinematic chain made control complicated and the low stepping frequency in an MRI environment made the robot too slow.

In 2017, the Stormram 4 was presented (Fig. 22.4, left). This system has a serial kinematic manipulator with four DoFs, of which two are driven by curved stepper motors and two by linear stepper motors. With a compact size of 72 × 51 × 40 mm (excluding racks) this robot combines a relatively large workspace with good accuracy, still at low speed in the MRI environment [23,24]. In the following year the Sunram 5 was developed (Fig. 22.4, right) which utilizes dual-speed motors on certain axes. The Sunram 5 has five DoFs driven by a total of six stepper motors and also includes a breast fixation system, a pneumatic biopsy gun, and a safety needle ejection mechanism [25].

All stepper motors used in Stormram 1–4 and Sunram 5 consist of two or three double-acting cylinders that engage on a straight or curved rack by means of a wedge mechanism [26,27]. The rectangular-shaped cylinders allow efficient stacking of multiple cylinders within a single housing. This is particularly useful for the two dual-speed motors in

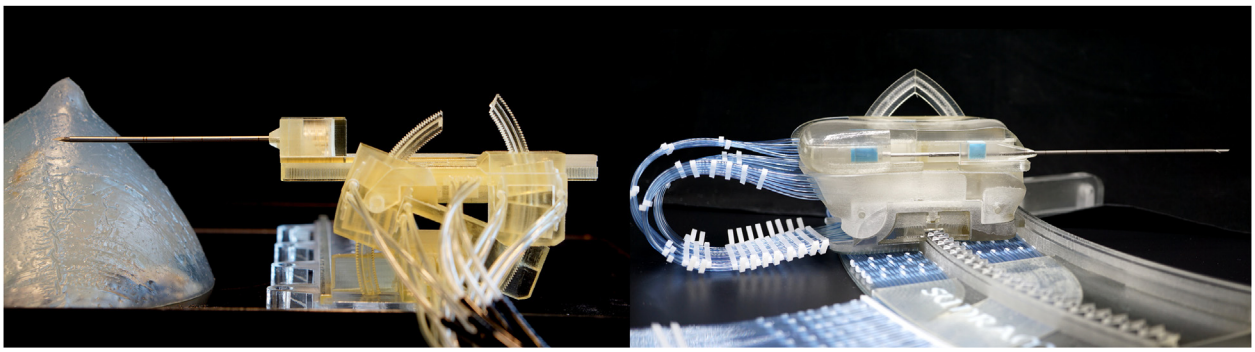

FIGURE 22.4 Stormram 4 (left) and Sunram 5 (right).

Sunram 5 in which four or five cylinders are positioned in line, enabling both large-step and small-step movements in the same movement direction [28].

The minimum required number of DoFs in a biopsy robot is three: the location of a lesion is represented as a point in space while the needle insertion direction can in principle be chosen arbitrarily. Additional DoFs are useful in order to navigate around impassable structures: examples are the grating of the breast fixation system and any anatomical features indicated by the radiologist that should be avoided. With five DoFs Sunram 5 has sufficient dexterity to circumvent such structures and reach difficult locations in the breast.

22.1.5 Organization of the chapter

The remaining sections of this chapter are organized as follows: Section 22.2 describes the design and manufacturization of single-acting cylinders, Section 22.3 describes linear and curved stepper motors and dual-speed motor concepts, Section 22.4 describes the design and kinematics of Sunram 5, Section 22.5 describes control methods for cylinders, stepper motors, and robotic systems, Section 22.6 describes evaluation methods and experimental results of stepper motors and the Stormram 4, and finally Section 22.7 wraps up the chapter.

22.2 Pneumatic cylinders

This section describes the principles, design, and production aspects of pneumatic cylinders. The single-acting cylinder is presented as an example as this is the easiest to design, manufacture, and evaluate. The necessary files for 3D printing and laser-cutting this device are available for download [29].

Pneumatic cylinders consist of a hollow cavity in which a piston can slide back and forth. When a pressure P is applied in the cavity at one side of the piston, a force $F = P \cdot A$ is exerted on its surface A which may result in motion, delivering work to the environment. By alternatingly applying pressure to either side of the piston through separate pneumatic connections, the piston can be moved back and forth pneumatically and this is called a double-acting cylinder.

22.2.1 Rectangular cross-sectional shape

Most traditional cylinders have a circular cross-section. The main reasons are that circles have an optimal area/circumference ratio, allowing cylinders to be produced with relatively thin walls. Also, circular holes can be easily manufactured by conventional drilling techniques and the absence of sharp corners in the walls makes sealing relatively easy. On the other hand, cylinders with circular walls are much more difficult to manufacture precisely using 3D printing techniques than cylinders with straight walls due to characteristics involved in 3D printing. More specifically, the additive manufacturing techniques that deposit filament layer-by-layer result in staircase effects and poor surface finish at steep overhangs, present in horizontally oriented cylindrical cavities. In vertically oriented cylindrical cavities the layered structure also causes difficulties in motion and sealing. In order to circumvent these drawbacks, box-shaped cylinders are used in this chapter. Its cross-sectional area is rectangular and the structures can be manufactured with good accuracy. An additional advantage is that a rectangular cylinder makes more efficient usage of the available space than circular cylinders with the same wall thickness.

No protruding cylinder rods are used in the double-acting pneumatic cylinders. While it would be possible to use such rods with appropriate sealing, different methods are used to transfer work to the environment. In the case of stepper motors, interaction between pistons and racks occurs by means of teeth positioned between the two heads of each piston.

22.2.2 Sealing

A piston moves inside a cylinder as a result of pressure being applied to one of its surfaces. This pressure is supplied by a pressure source through a valve manifold outside the MRI room. It is essential that pressure is transferred as effectively as possible, so leakage in the cylinder must be kept to a minimum in order to avoid pressure drops. Without proper sealing a significant amount of leakage would occur through the gap between the piston and the cylinder walls; this gap is necessarily present to allow the sliding motion of the piston inside the cylinder.

Elastomer O-rings as used in circular cylinders do not function in rectangular cylinders due to the four right-angled corners which the O-ring cannot cover. Instead, plates of silicone rubber with thickness 0.5−1.0 mm are chosen as the sealing material. A laser cutter is used to cut rectangular pieces out of it. Alternatively, the seals can be cut by hand using a cutting tool. The seal width and height should be approximately 0.2−0.3 mm larger than the respective cylinder cross-sectional dimensions to ensure good sealing without causing excessive friction.

The seal edges need to be slanted at an angle of 2−15 degrees. This implies that the seal faces are not equal: one side has a larger surface area than the other. For effective sealing the larger face must be oriented toward the air chamber, while the smaller face touches the piston head. When pressurized air acts on the larger surface of the seal it effectively pushes the seal edges against the cylinder walls resulting in a proper sealing function.

In most cases it is not necessary to fixate the seals to pistons mechanically. The sufficient condition is that the piston is only moved pneumatically and not by external forces, which guarantees that the seals are pressed against the piston heads at all times and will not become detached.

22.2.3 Design of the single-acting cylinder

The development of a new pneumatic actuator using the technology described in this chapter is an iterative process. In order to study the dimensional aspects of the cylinder parts and how to seal it properly, it is useful to design and build the open single-acting cylinder shown in Fig. 22.5. This design allows to explore different sealing techniques and part dimensions in order to obtain the right tolerances experimentally, as the piston and seal can be taken out even after gluing the housing. It also allows to evaluate the piston forces and air leakages at a range of pressures. The presented techniques can subsequently be applied to create rectangular-shaped cylinders of any size.

The shown cylinder has a cavity of $12 \times 10 \times 10$ mm and walls of 2 mm. This results in outer dimensions of $16 \times 14 \times 12$ mm, excluding the pneumatic socket which is a 2-mm hole with depth 4 mm. The theoretical output force at a pressure of 0.4 MPa is $(0.4 \cdot 10^6 \text{Pa}) \cdot (12 \cdot 10^{-3} \cdot 10 \cdot 10^{-3}\ \text{m}^2) = 48$ N.

The cylinder is printed in two parts: a housing and a cap. The piston has a head which covers the cross-sectional area with a small clearance (order of 0.1 mm), to allow for smooth movements without wobbling. In Fig. 22.5 a solid block is used as a piston, but in practical applications the piston may include features to interact with the environment. The seal is also rectangular, but must be slightly larger than the cross-sectional area of the cylinder: typical dimensions are $12.3 \times 10.3 \times 0.5$ mm. The cross-sectional area can be reduced if friction is too high, or increased in case of (excessive) leakage. A thicker seal (e.g., 1 or 1.5 mm) allows for more rigidity which may be useful in cylinders larger than 15 mm in size.

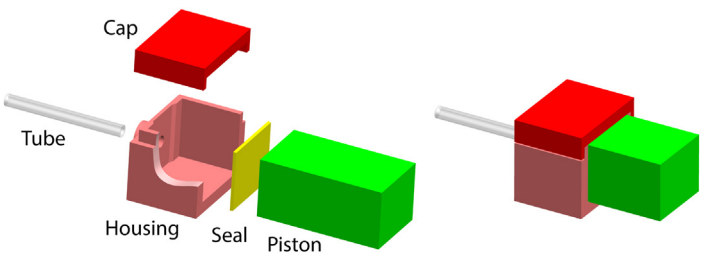

FIGURE 22.5 Exploded (left) and assembled (right) views of single-acting cylinder design, with housing (*red*), piston (*green*), and seal (*yellow*).

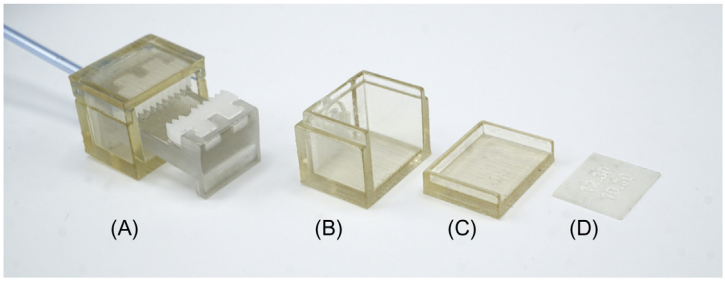

FIGURE 22.6 Realization of single-acting cylinder. (A) Assembled cylinder with piston, (B) housing, (C) cap, (D) seal.

22.2.4 Manufacturization

The presented pneumatic cylinders and pistons are printed on a Polyjet printer (Connex3 Objet260, Stratasys Ltd., Eden Prairie, MN, United States) in VeroClear material, standard quality, glossy finish. The glossy finish option implies that the top surfaces and side walls of the part are not covered with support material, which is important as supported faces are relatively rough and would cause excessive friction.

As shown in Fig. 22.5 (left), the cylinder is printed in two pieces: the housing and the lid. Fig. 22.6B and C shows these parts in the preferred print orientation which ensures that all four cylinder walls are printed with a glossy finish. Furthermore it is advisable to orient the parts such that the print head moves in the same direction (along the *X*-axis of the printer) as the piston would do in the cylinder, in order to obtain the smoothest possible finish for the cylinder walls along the direction of movement.

The next step is to join the parts together. Screws are not a good option in small-scale MR-safe applications due to space constraints, so bonding by glue (e.g., cyanoacrylate) is used. The challenge is to create an airtight bond without excess glue entering the cylinder cavity. It is therefore important to apply the right amount of glue and also to operate the cylinder at very low pressure right after assembly. In closed cylinder designs it is also recommended to cover the piston and seal in petroleum jelly (Vaseline) before gluing the housing together. Besides serving as a lubricant, it also allows the seal to wipe away excess glue inside the housing before the glue has hardened out. A light patch of blue silicone (Loctite 5926) on the cylinder edge may be useful to improve the airtightness and reduce the risk of jamming.

Polyurethane tubes can be glued to the housing using cyanoacrylate (Loctite 406). An activator such as Loctite 770 should be applied to the polyurethane parts before gluing to ensure a good bond.

See Fig. 22.6A for the resulting single-acting cylinder with a typical piston. The piston can be pushed in by hand and pushed out by pressurized air. The amount of leakage and friction can be qualitatively assessed by hand and quantitatively studied using appropriate equipment. Based on the cross-sectional area, every 0.1 MPa ($\approx$1 bar) of pressure approximately results in an additional 12 N ($\approx$1.2 kg) of force.

22.2.5 Double-acting cylinder

A single-acting cylinder can push a piston in one direction only. In most applications a return stroke mechanism is required. In our applications a second single-acting cylinder is most suited for this. Alternatives are a mechanical (or permanent pneumatic) spring which requires fewer pneumatic tubes, but this results in much smaller net output forces for a given cross-sectional area.

The combination of two single-acting cylinders opposite each other results in a double-acting cylinder. The cross-sectional area of the two opposite bores can be the same or different depending on the specific application. The piston is a single rigid object with two piston heads and no protruding rod. The specific piston shape defines the way it interacts with the environment, such as engaging with a toothed rack or firing a biopsy gun.

22.3 Stepper motors

A pneumatic stepper motor can be constructed from two or three double-acting cylinders that act on a toothed rack (or gear). In the two-cylinder version (Fig. 22.7) the rack and pistons have teeth on two sides, while in the three-cylinder version (Fig. 22.8) only one side is toothed.

The two-cylinder stepper motor design has four distinct states, shown in Fig. 22.7. In each state both cylinders act on the rack, but only one of them can be fully engaged on it, which is always the piston that moved formerly. The consequence is that there is no backlash, but a hysteresis is present: when reversing direction, the observed rack position

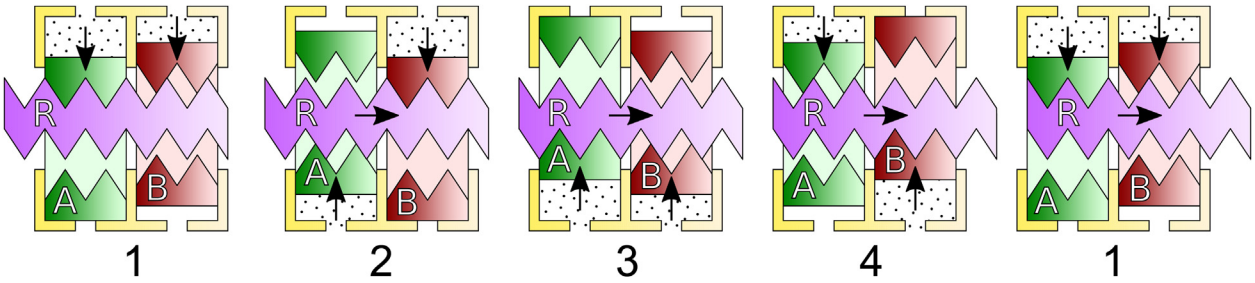

FIGURE 22.7 (1−4) Sequence of states in a two-cylinder pneumatic stepper motor, with rack moving from left to right. The rightmost state is identical to the leftmost one, but with the rack displaced to the right by one tooth pitch.

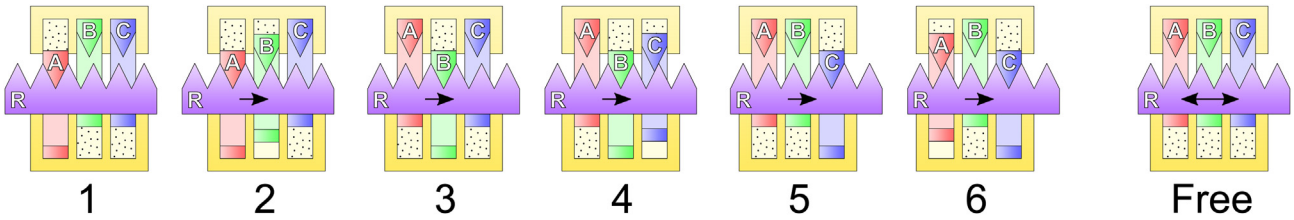

FIGURE 22.8 (1−6) Sequence of states in a three-cylinder pneumatic stepper motor, with rack moving from left to right. The "free" state (right) is the free-running state in which all pistons are moved up.

includes a certain offset compared to those in a forward direction. While this offset can be measured and accounted for, a simpler method is to approach each setpoint in a consistent (e.g., forward) direction.

The three-cylinder stepper motor design has eight distinct states, of which seven are shown in Fig. 22.8. (The eighth one, with all pistons engaging on the rack, is of no practical value.) In states 1, 3, and 5 exactly one piston engages on the rack and backlash may be present due to the finite clearance between piston and cylinder walls. In states 2, 4, and 6 the backlash is eliminated at the cost of the introduction of hysteresis like in the two-cylinder stepper motor design. Unlike in the two-cylinder design there is a free-running state, which allows to move the rack by external forces with negligible resistance.

22.3.1 Design of the two-cylinder stepper motor

Like pneumatic cylinders, stepper motors come in various sizes. One specific design of a two-cylinder stepper motor is presented as an example and the associated files are available for download [29]. Fig. 22.9 shows a rendering of this stepper motor, which has dimensions $32 \times 30 \times 16$ mm (excluding the rack). It consists of a housing with two top cover plates, two pistons, a rack, and four seals. The cylinder cross-sectional area is 12×10 mm and the teeth pitch of this particular design is 1.2 mm, resulting in a step size of 0.3 mm. The separation between the cylinders needs to be such that the cylinder pattern spacing is an odd multiple of the step size, as visualized in Fig. 22.7. In this case it is $47 \cdot 0.3$ mm $= 14.1$ mm, resulting in a central wall thickness of $14.1 - 12$ mm $= 2.1$ mm.

In this stepper motor design the piston teeth are constructed by laser-cutting a 2 mm acetal plate. The advantages of laser-cut teeth are sharper tips, increased strength, lower friction, and reduced wear. These parts are inserted in the appropriate slots of the pistons and interact smoothly with the 3D printed teeth of the rack.

Fig. 22.10 shows a realization of the stepper motor. The production and assembly process is similar to that of the single-acting cylinder. Again, the parts are printed in VeroClear, glossy finish, cylinder walls facing up and aligned with the *X*-axis of the polyjet printer. The air vents are initially filled with support material, but easily cleared with a small wire and the use of an air gun. Silicone grease (Vaseline or equivalent) is used as lubricant, blue silicone acts as sealant, and cyanoacrylate is used to glue the two caps to the housing. After assembly the cylinders are briefly operated at low pressure (without rack) to clear the cylinder walls from excess blue silicone and/or glue before hardening out while holding the housing together using clamps. After the glue has hardened out, the rack can be carefully inserted while slowly operating the cylinders at low pressure; some grinding and/or lubrication may be required to allow smooth movement of the rack. Finally the pressure can be increased to 0.1−0.4 MPa or higher.

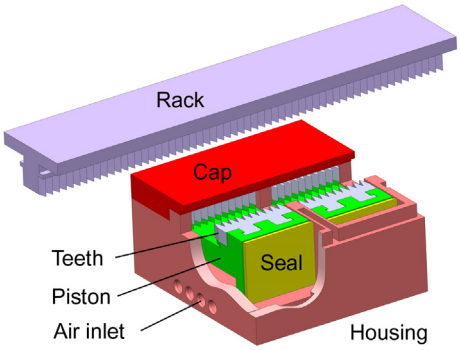

FIGURE 22.9 Cut-out view of small-step two-cylinder linear stepper motor.

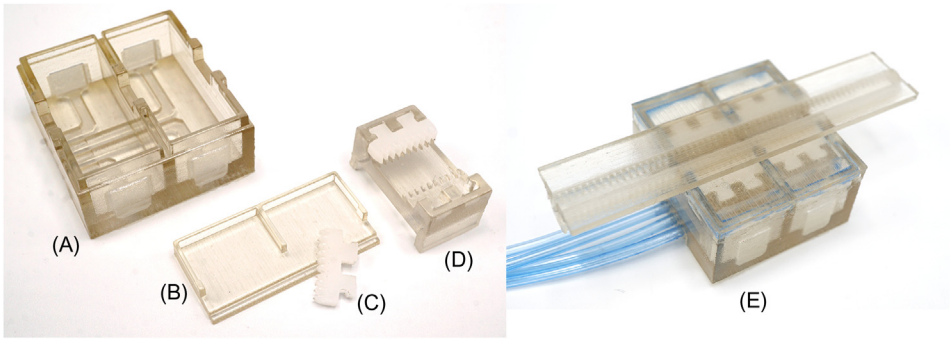

FIGURE 22.10 Realization of small-step two-cylinder linear stepper motor: (A) housing, (B) one cap, (C) laser-cut teeth piece, (D) piston with one teeth piece inserted, and (E) assembled motor.

22.3.2 Curved stepper motor

The rack of a stepper motor does not need to be linear: it can also follow a circular arc with some (finite) radius R. In fact, a linear stepper motor is a special case having $R = \infty$.

Fig. 22.11 shows the design of a two-cylinder curved stepper motor. The two cylinders are not parallel, but angled in order to keep the piston movement perpendicular to the curvature of the rack. Apart from this, the design principles are the same as those of the linear stepper motors.

The piston teeth should be shaped such that they interact with the rack teeth at the same moment and minimize the risk of jamming. Fig. 22.12 shows details of the teeth shapes in two positions of the piston and rack. The rack teeth are straight and symmetrical, while the piston teeth are slightly curved for two reasons. The first reason is made clear in Fig. 22.12A, in which it can be observed that the optimized piston teeth tips all make contact with the rack at the same moment so that load forces are as evenly distributed over all teeth as possible. The second reason is apparent in Fig. 22.12B. With the piston fully engaged on the rack, the nonengaging teeth tips must be opposite to the rack teeth (shown in *dotted lines*). This ensures that all piston teeth engage with the rack in a consistent manner, that is, all pushing the rack to the left or all to the right. A nonoptimized piston teeth shape (*dashed lines*) would have the possibility of jamming, making the motor less reliable.

22.3.3 Dual-speed stepper motor

In an MRI environment the stepping frequency is limited to approximately 10 Hz when full force is needed. This would result in long procedure times when large distances are to be covered with high accuracy. A straightforward solution is to combine two (or more) stepper motors together on the same axis, allowing for both high-speed and high-accuracy movements.

A dual-speed stepper motor is essentially a combination of two singular stepper motors with different step sizes arranged in a serial kinematic chain. In order to make efficient use of the space, each dual-speed motor consists of a single housing in which cylinders for all pistons of both singular stepper motors are arranged in line. The two racks are positioned at opposite sides of the housing. This way the cross-sectional area of the dual-speed motor is the same as in the single-speed motor, while the extra length in the housing only occupying space in the direction of movement.

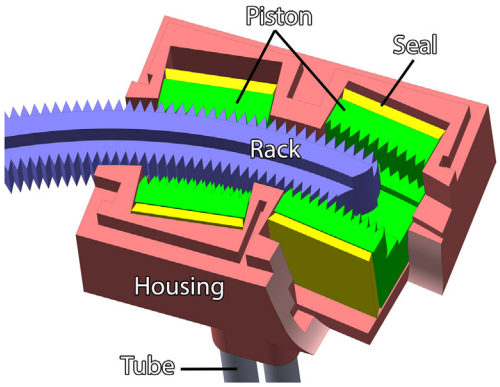

FIGURE 22.11 Cut-out view of a curved stepper motor, exposing the two pistons, four seals and rack in the housing.

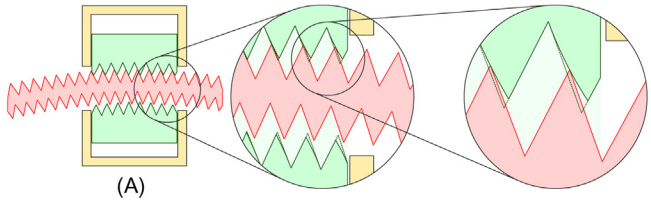

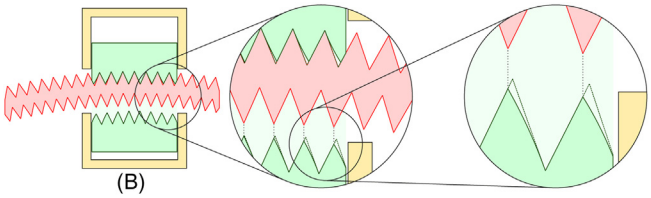

FIGURE 22.12 Analysis of teeth shape in curved stepper motor. The piston teeth have a special shape in order to optimize contact and reduce risk of jamming.

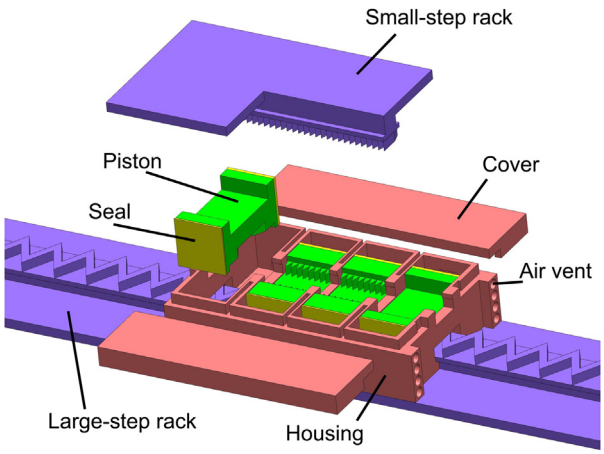

FIGURE 22.13 Dual-speed stepper motor design. The top rack has pitch 0.3 mm, the bottom rack has pitch 1.7 mm.

The key design aspect is the pitch sizes of both singular motors. The most straightforward approach is to combine a large-step motor for fast movements with a small-step motor for high accuracy. An alternative approach is to use two large-step motors with slightly different step sizes, exploiting the step size difference to making small steps.

Fig. 22.13 shows the design of a generic dual-speed motor with size $50 \times 32 \times 14$ mm (excluding racks). It consists of four pistons: the outermost two pistons operate the large-step rack with step size 1.7 mm, while the innermost pistons operate the small-step rack with step size 0.3 mm. Measurements have shown that the maximum force under load is 24 N at a pressure of 0.3 MPa, and positioning accuracy is 0.1 mm [28].

22.4 Design of Sunram 5

This section describes the kinematics and mechanical design of Sunram 5. It is driven by linear and curved stepper motors, dual-speed motor combinations, and single-acting and double-acting pneumatic cylinders described earlier in this chapter. The actuators are specifically adapted to the needs of the respective axes. First the kinematic configuration is described, followed by details of the mechanical implementation.

22.4.1 Kinematic configuration

Fig. 22.14 shows the kinematic configuration of Sunram 5. Fig. 22.15 shows a photo of the Sunram 5 indicating the movement directions of the joints and cylinders.

Joint $J1$ is a curved stepper motor with a radius of 260 mm. The teeth pitch is 1.5 degrees, equivalent to a teeth distance of 6.81 mm and a step size of 1.7 mm along the curved rack. The total range is 35 degrees (93 steps). It is used for coarse positioning of the robotic system and the curvature allows for a more favorable insertion angle near the borders of the workspace compared to pure linear motions. Joint $J2$ is a linear stepper motor with step size 0.3 mm and a range of 45 mm (150 steps). Joint $J2$ is used for fine lateral adjustments, but can also be used in conjunction with $J1$ to tilt the needle sideways over small angles to circumvent the grating of the breast fixation system and/or optimize the needle trajectory. Although joint $J1$ and $J2$ operate on different axes, the combination has characteristics of a

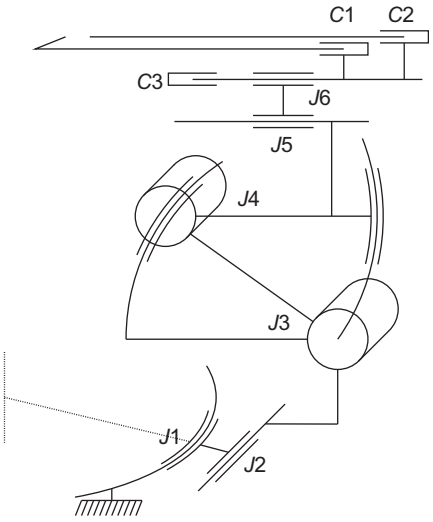

FIGURE 22.14 Kinematic configuration of Sunram 5 with joints $J1-J6$, biopsy gun cylinders $C1$ and $C2$, and emergency ejection cylinder $C3$.

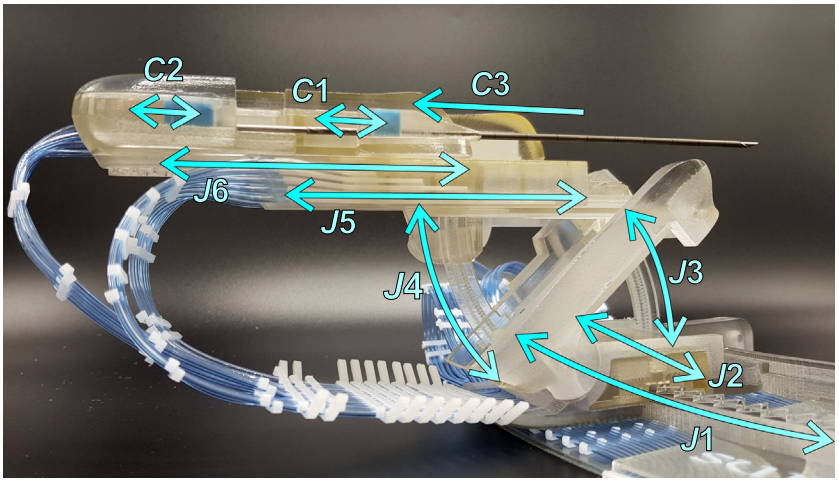

FIGURE 22.15 Photo of Sunram 5 with movement directions of joints $J1-J6$ and cylinders $C1-C3$.

dual-speed stepper motor because of the capability of both quick and precise lateral positioning over the full width of the workspace.

Joints *J*3 and *J*4 are rotational stepper motors that lift and tilt the needle holder vertically. Both joints *J*3 and *J*4 are single-speed curved motors with a radius of 62 mm and teeth pitch of 1.2 degrees corresponding to a step size of 0.3 degree (0.32 mm at 62 mm) and a range of 40 degrees (133 steps).

Joint *J*5 is a linear stepper motor which moves the needle holder assembly forwards and backwards in small steps. The pitch size is 1.2 mm corresponding with a step size of 0.3 mm and the range of motion is 50 mm (167 steps). Joint *J*6 is a three-cylinder linear stepper motor with pitch size 5.1 mm, step size 1.7 mm, and range of motion of 61 mm (48 steps) along the same axis as *J*5, so joints *J*5 and *J*6 together form a true dual-speed stepper motor.

Cylinder *C*1 drives the inner needle of the biopsy gun forward over a distance of 19 mm and cylinder *C*2 slides the needle shaft over the inner needle over the same distance. Cylinder is *C*3 is the emergency needle ejection cylinder and it is effective when joint *J*6 is in free-running state.

22.4.2 Mechanical design of Sunram 5

Fig. 22.16 shows two 3D computer-aided design (CAD) drawings of the Sunram 5, in compact and extended configurations. The robot consists of 16 pneumatic cylinders in total, distributed over six singular stepper motors, two double-acting cylinders and one single-acting cylinder. The height of each cylinder is 10 mm and the nominal wall thickness is 2 mm. With the exception of joints *J*3 and *J*4, all cylinders are oriented horizontally and distributed across three levels of approximately 14 mm each. This results in a total height of only 47 mm for the moving part of the Sunram 5 robot (excluding racks and cable guide).

Fig. 22.17 shows the actuators of joint *J*1 and *J*2. The motor design and cylinder arrangement are similar to that of the dual-speed stepper motor shown in Fig. 22.13. The only significant difference is that joint *J*1 is slightly curved with

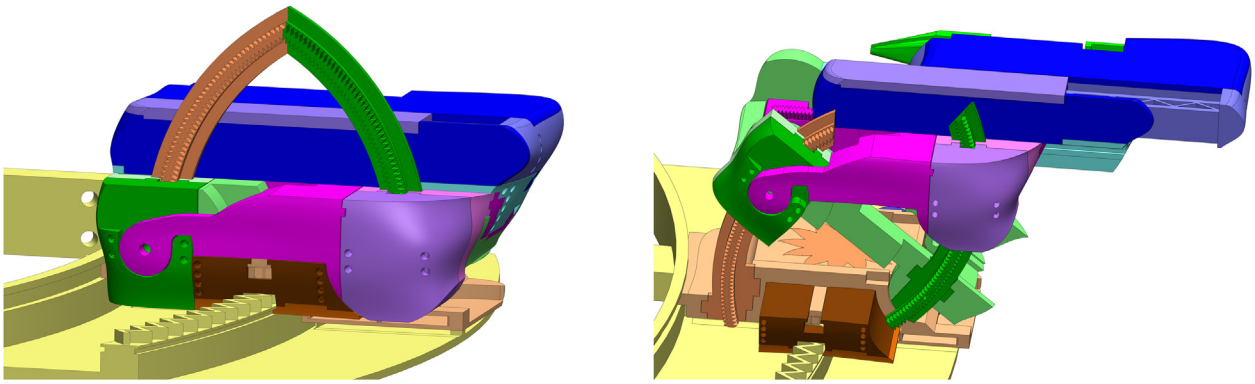

FIGURE 22.16 Computer-aided design (CAD) drawing of Sunram 5, in compact (left) and extended (right) configurations.

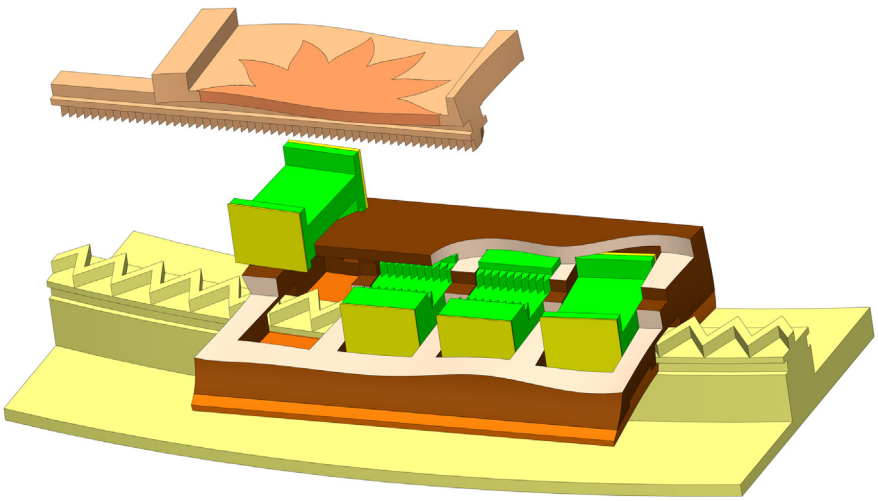

FIGURE 22.17 Actuators of joints *J*1 and *J*2 to drive the Sunram 5 sideways along the track. The curved bottom rack has step size 1.7 mm along the rack, the top rack has step size 0.3 mm.

curvature radius 260 mm, resulting in the outermost two cylinders being angled respective to the other cylinders. The small-step rack (joint $J2$) is connected to the base with a guiderail as shown in Fig. 22.16, in order to reduce parasitic rotational movements in both $J1$ and $J2$.

Fig. 22.18 shows a cross-section of joints $J3$ and $J4$ that lift and tilt the Sunram 5 vertically. Both joints are curved stepper motors similar to the one shown in Fig. 22.11. The curved rack has a radius of curvature of 62 mm and the optimized teeth shapes of Fig. 22.12 are used in the pistons which are laser-cut from 2 mm acetal and attached to the 3D printed piston with small pins.

Acrylic pins with diameter 3 mm are used as passive hinges in the axis of rotation of joints $J3$ and $J4$. These pins are partially visible in Fig. 22.15 and greatly reduce the amount of parasitic movements in the kinematic chain. Moreover, the hinge of either joint coincides with the curved rack of the other joint, resulting in a truss-like mechanical structure in extended configuration.

The needle insertion mechanism consists of one dual-speed stepper motor, one single-acting emergency ejection cylinder, and two dual-acting biopsy gun cylinders.

The dual-speed motor is shown in Fig. 22.19. It consists of a three-cylinder large-step part with pitch size 5.1 mm and step size 1.7 mm, and a two-cylinder small-step part with step size 0.3 mm. The specific arrangement of the five cylinders allows for a telescopic expansion as shown in Fig. 22.15. This expansion is needed to allow sideways movements of the Sunram 5 with the 100 mm biopsy needle installed, without colliding with the frame of the breast fixation system.

Fig. 22.20 shows the emergency needle ejection and biopsy gun mechanisms. A single-acting cylinder with dimensions 13×10 mm is used for the ejection mechanism and is connected to the needle motor's large-step rack as shown in Fig. 22.21. The ejection mechanism can be activated whenever the three pistons of the large-step needle stepper motor (Fig. 22.19) are all retracted ("Free" state in Fig. 22.8).

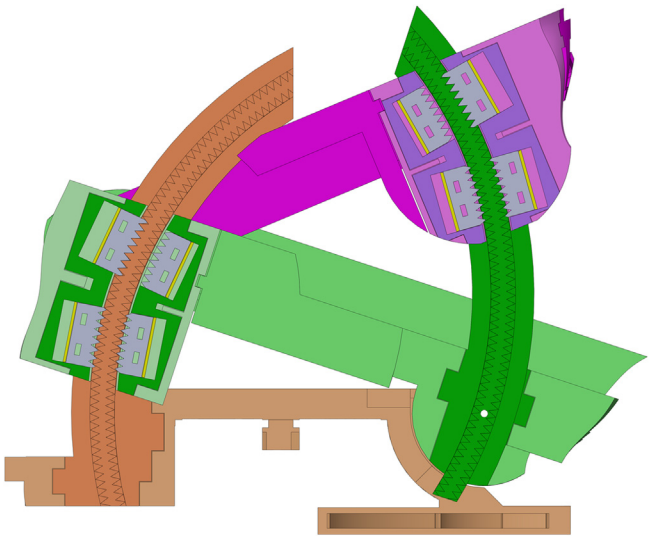

FIGURE 22.18 Cross-sectional picture of joints $J3$ and $J4$ which lifts and tilts the Sunram 5 vertically.

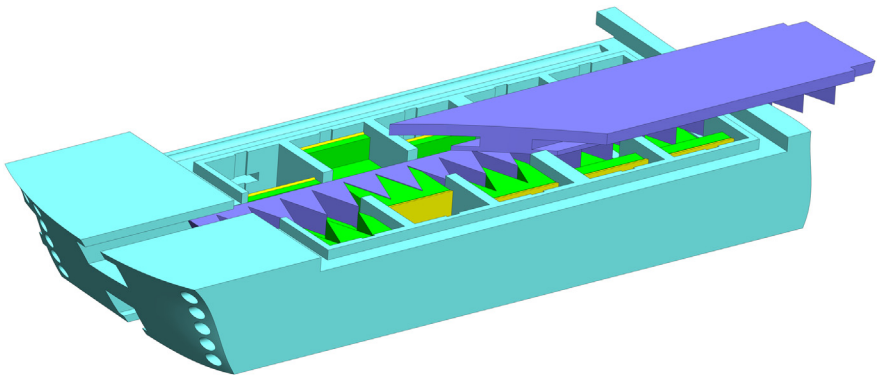

FIGURE 22.19 Cut-out view of Sunram 5's dual-speed needle insertion motor. The three cylinders in front operate the large-step rack on top with step size 1.7 mm.

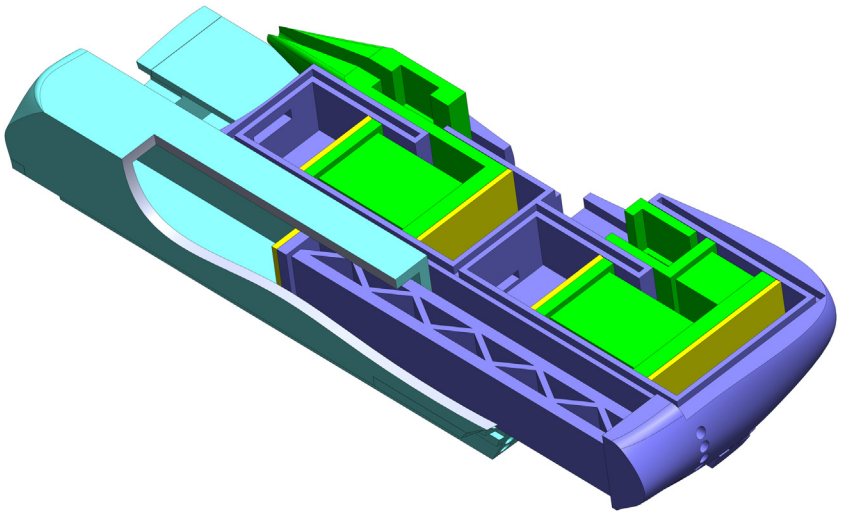

FIGURE 22.20 Cut-out view of Sunram 5's emergency eject single-acting cylinder (left) and the two dual-acting pneumatic cylinders for the biopsy gun (right).

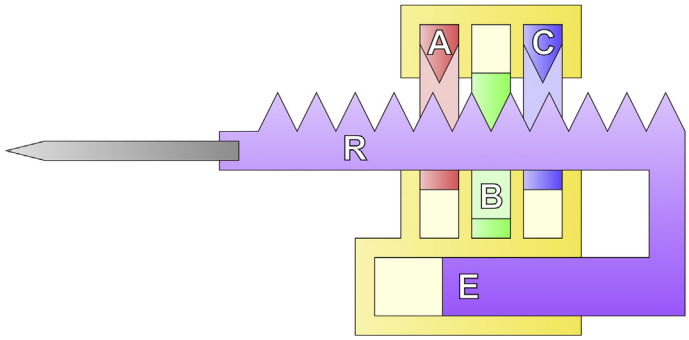

FIGURE 22.21 Needle safety mechanism. Pistons A, B, and C together with rack R form a three-cylinder stepper motor, while piston E (connected to rack R) is part of a single-acting cylinder.

The biopsy gun consists of two double-acting cylinders. Its respective pistons have a smaller and a larger piston head and this asymmetry allows to attach needle sockets to the side of each piston in a compact design. The stroke of both cylinders is 19 mm and the total length of the biopsy gun is approximately 100 mm.

22.5 Control of pneumatic devices

Each pneumatic cylinder is controlled individually by one 5/2-way valve of type Festo MHA2-MS1H-5/2-2 (Festo AG and Co. KG, Esslingen, Germany), located in the valve manifold of the controller located outside the Faraday cage of the MRI scanner. The valve is a high-speed solenoid valve with nominal airflow 100 L/min and a specified switching time of 1.9 ms. The use of more conventional internally piloted valves such as PV5211-24VDC-1/8 (TechniComponents B.V., Waalwijk, The Netherlands) is also possible. In an MRI environment the tube length should be around 5 m and its outer diameter can be 3−4 mm. In the Sunram 5 the last 0.5 m of the tube has a diameter of 2 mm in order to provide sufficient flexibility in the various DoFs. The cable bundle is managed such that it exits the robot at a fixed point in the frame (Fig. 22.22).

It is not recommended to use 2 mm tubes for the full distance between controller and robot as this would constrain the airflow too much, resulting in reduced output force at the same stepping frequency. Likewise, it is not recommended to use 6-mm tubes to connect the robot to the controller as the associated cable bundle would be quite big and the large volume of air inside the tubes would require the use of bigger valves and additional air supply capacity in order to provide sufficient airflow.

Sunram 5 contains 16 pneumatic cylinders with a total of 31 pneumatic connections (one cylinder is single-acting). It is theoretically possible to lower this number of tubes in different ways. Cylinders belonging to different stepper motors could share the same tube pairs, at the cost of increased controller software complexity and hysteresis effects. It is also possible to control a cylinder with a single pneumatic tube if full force is not needed. In that case a constant

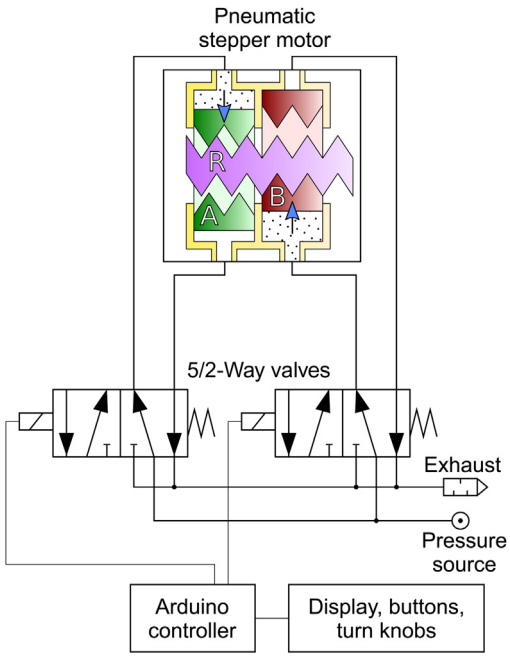

FIGURE 22.22 Schematic for controlling a two-cylinder stepper motor using two 5/2-way valves.

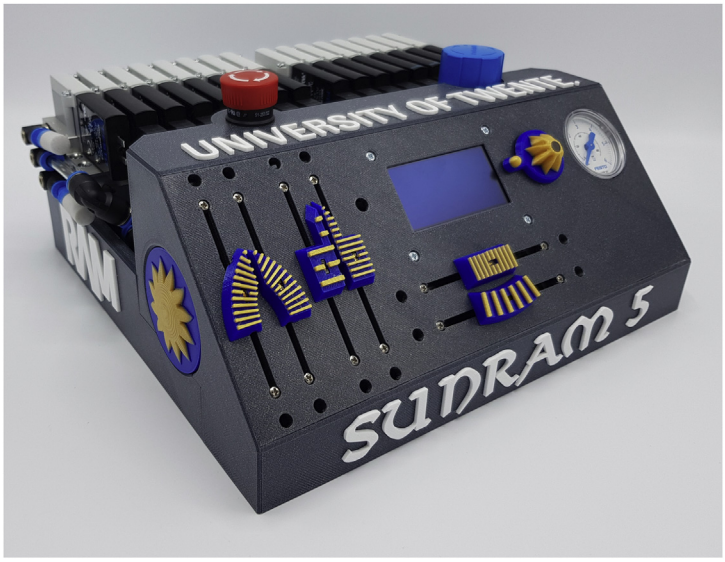

FIGURE 22.23 Sunram 5 controller with user interface.

return spring action must be present with (approximately) half the force of the active stroke. This could be provided by, for example, a constant pressurization of the other end at half the system pressure, or equivalently by pressurization of a smaller cylinder area at system pressure.

In Sunram 5 the pneumatic manifold is controlled by an Arduino microcontroller, which is in turn commanded by a user interface. Fig. 22.23 shows a photo of the controller. Besides the valves and Arduino controller it also includes a pressure adjustment knob with gauge, internal pressure tanks, an emergency stop button, six sliders for direct control of the stepper motors, a display for status information accessible by a menu dial, and a tristate biopsy fire switch. On the right panel there are connections for electric power, air supply, and universal serial bus (USB).

Feed-forward is used as the control method. This is sufficient provided that the initial position is known and no steps are skipped thereafter. The calibration process involves operating the robot to a predetermined position by either visual guidance or by operating each axis toward its endstops at low pressure (or high speed). In order to guarantee that no

steps are skipped after calibration, motor forces must exceed maximum joint load forces by a certain safety margin. A typical stepper motor in Sunram 5 is capable of exerting over 50 N at 0.5 MPa pressure, which is more than enough to insert a sharp needle in breast tissue. It is also possible to increase the stepping frequency beyond the bandwidth when executing free-air movements in order to minimize the total procedure time.

While it is certainly possible to incorporate incremental position encoding in an MR-safe robot using, for example, fiber optics, the associated complexity and additional space requirements are considerable. If additional space were available, it could also be used to increase the cylinder cross-sectional areas instead, leading to higher motor forces and reducing the necessity for positional encoders.

The presence of the robot inside the MRI scanner offers a potential indirect way of position feedback. By including suitable passive fiducials such as oil capsules in the robot design the relative location of the various linkages can be measured with submillimeter accuracy in a typical MRI scanner.

In the clinical workflow the breast is immobilized by a fixation system to which the robot is attached. Fiducials in the frame provide a way of defining the robot−MRI coordinate transformation, allowing to represent the target lesion in robot coordinates. After choosing the desired path trajectory by the radiologist, the joint configuration of Sunram 5 can be computed.

The specific serial kinematic design of Sunram 5 allows for straightforward computation of the joint configuration corresponding with the desired needle insertion trajectory. The needle lift/tilt and insertion mechanisms all move the needle in the same vertical plane, so the first step is to align that vertical plane with the target lesion by choosing appropriate joint coordinate values for joints $J1$ and $J2$. The next step is to calculate the joint coordinate values for joints $J3$ and $J4$, aligning the needle holder with the lesion. Finally, joint coordinate values for joints $J5$ and $J6$ are calculated based on the distance from needle tip to lesion. The biopsy gun can now be fired and the needle with the specimen extracted.

22.6 Evaluation of stepper motors and Stormram 4

Stepper motors can be characterized by finding the relation between output force, system pressure, and stepping frequency. In a full robotic manipulator such as the Sunram 5, relevant characteristics are the needle tip positioning accuracy and precision and the average travel time in an MRI environment.

22.6.1 Stepper motor force

Sunram 5 consists of several cylinders and stepper motors. The theoretical output force of a pneumatic piston can be calculated from its cross-sectional area multiplied by the system pressure. The interaction of a piston with a straight or curved rack by means of the wedge mechanism results in a transfer of force with a specific leverage, as determined from the teeth pitch and depth. The actual output force is lower due to friction in the sliding parts and can be measured.

Fig. 22.24 shows the schematic setup for evaluating the stepper motor force as function pressure and stepping frequency parameters. A set of masses with known weights is used to generate forces, transferred to the motor by means of a rope over a pulley. The pressure is adjusted to the lowest level that the motor can still lift the given masses without skipping steps.

Fig. 22.25 shows a photo of an actual setup and Fig. 22.26 shows the pressure−force graph for this specific motor. It can be observed that there is a good linear relationship between pressure and force, with a maximum of 62 N at a pressure of 0.65 MPa. Given the cylinder cross-sectional area of 10×10 mm and the leverage factor of 2.4, this results in a mechanical efficiency of 43% [23].

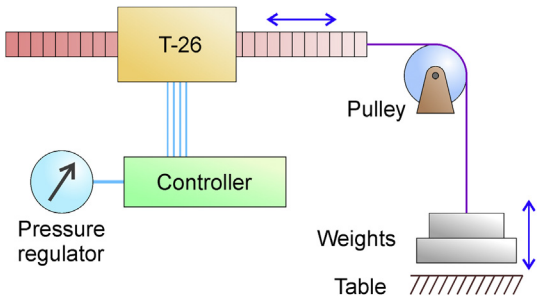

FIGURE 22.24 Schematic setup for stepper motor force measurements.

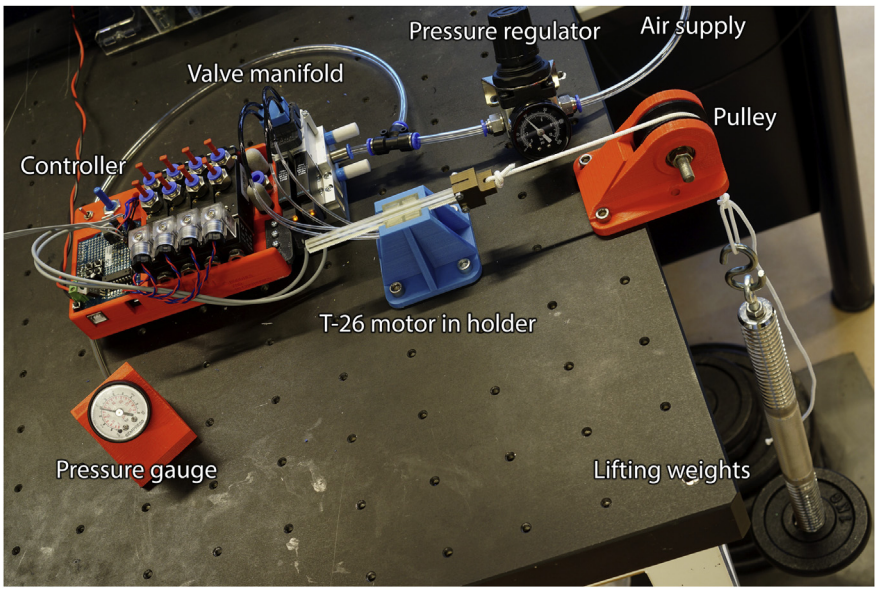

FIGURE 22.25 Photo of force measurement setup for T-26 stepper motor.

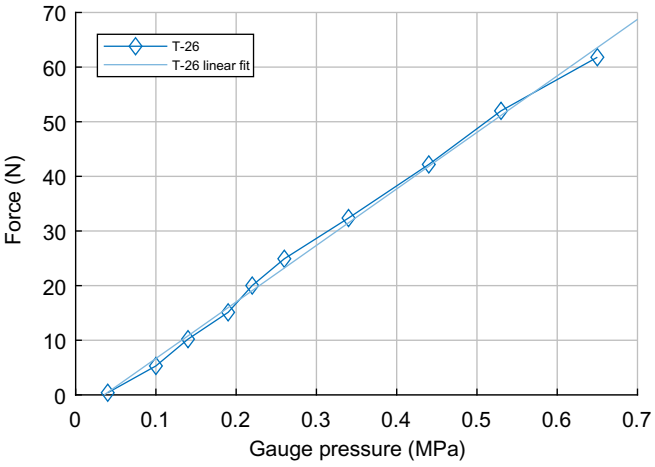

FIGURE 22.26 Pressure−force graph for the T-26 stepper motor.

At a relatively low pressure of 0.15 MPa, the force of 11 N is already large enough to move a Sunram 5-like robot along all its axes, except for inserting the needle through relatively stiff tissue for which more pressure is needed.

Besides this motor, the authors of this chapter earlier analyzed and reported about 10 different individual stepper motor implementations with mechanical efficiencies ranging from 22% to 76% [20,26,28]. Relatively low efficiencies (22%−34%) were found for the Stormram 1 motors which have cylinder cross-sectional dimensions of 20×4.1 mm. Its 5:1 aspect ratio results in a relatively high perimeter per surface area ratio and the low height of 4.1 mm makes effective sealing challenging [20]. This issue is solved by focusing on square-shaped cylinders with comparable width and height in all subsequent designs.

Another case of low measured efficiency (24%) was found in certain motors with 3D printed teeth with small pitch size (1.2 mm or smaller). Examination under a microscope reveals that the associated teeth tips are rounded, as shown in Fig. 22.27 (left), resulting in a reduced leverage factor and increased risk of jamming [28]. This issue is solved by using laser-cut teeth in the pistons and/or the rack, which result in sharper tip shapes as shown in Fig. 22.27 (right).

22.6.2 Stepping frequency

The maximum stepping frequency is another important characteristic and this is mainly dependent on the tube length (approximately 5 m in an MRI environment). Measurements have shown that the bandwidth is approximately 10 Hz

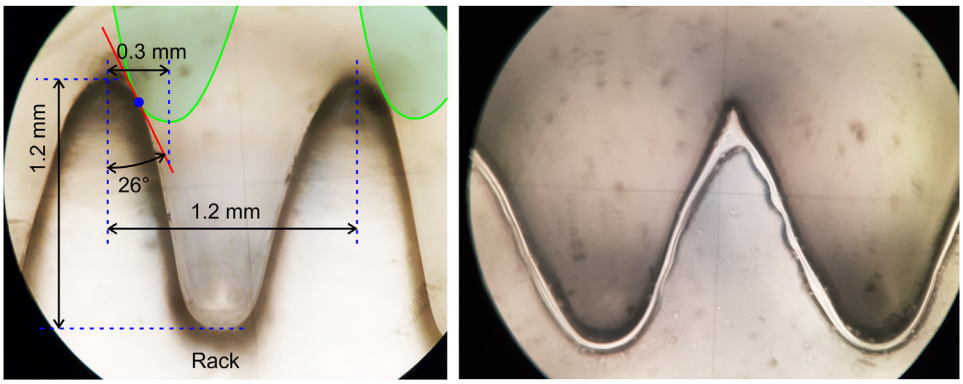

FIGURE 22.27 3D printed (left) and laser-cut (right) teeth with pitch size 1.2 mm, as seen under a microscope.

[26]. One factor is the limited speed of pressurized air in the tubes which cannot exceed the speed of sound (343 m/s) and is further restricted by the friction in the tubes. Another important factor is the finite volume of air inside the tubes (24.5 mL when using 4-mm tubes with 2.5 mm inner diameter), which implies that any further increase in tube thickness (to reduce wall friction) would require the use of larger valves with larger orifices. Nevertheless, the stepper motors in Stormram 4 have been shown to be able to operate at frequencies up to 65 Hz when moving in free air, as full force is not needed there.

22.6.3 Accuracy

Positional accuracy and overshoot have been studied for several stepper motors. Measurements have shown that hysteresis is present in two-cylinder stepper motors, with a magnitude of 60%−80% of the step size. The positional accuracy depends on the step size due to discretization: by design, the lower bound is half the step size in a singular stepper motor. In dual-speed stepper motors the accuracy can be as good as 0.1 mm [28]. The repeatability or precision is very good in general, measured to be as good as 0.01 mm [26].

22.6.4 Stormram 4 evaluation

Stormram 4 is the predecessor of Sunram 5. While it does not have the dual-speed motors that Sunram 5 has, the kinematic design is comparable and its measurement results give insights into the projected capabilities of Sunram 5.

Fig. 22.28 shows the experimental setup for evaluating the accuracy and precision of Stormram 4 in free air. Stormram 4 was programmed to approach all 35 targets in succession by navigating through a sequence of predefined way-points. Afterwards the offsets of each puncture from its respective target were measured. The average precision was found to be 0.71 mm in a horizontal direction and 0.21 mm in a vertical direction. Also, a bias of 1.0 mm was found in the horizontal direction due to manufacturing and/or calibration inaccuracies [23].

Fig. 22.29 shows the experimental setup for accuracy measurements inside a 0.25 T (G-scan, Esaote SpA, Genoa, Italy) MRI scanner. The Stormram 4 was mounted on a table with 10 fiducials in it. A polyvinyl chloride (PVC) phantom was placed on the table, a preoperative scan was made, and a series of 30 targets inside the phantom were selected. For each target, first its MRI coordinates were transformed to the robot coordinate frame as defined by the positions of the fiducials, after which a suitable joint coordinate vector was calculated. The robot, which had been calibrated previously in its zero-position, was then operated through a user interface by rotating the turn knobs corresponding with each joint manually until the displayed joint coordinates matched the target coordinates. A confirmation scan was then taken and automatically segmented to reconstruct the needle tip location and measure the distance to the target coordinates. Tissue deformations were left out of scope in the experiment as no fixation system was used.

Fig. 22.30 shows an example confirmation scan after applying geometric distortion correction. The 10 fiducials in the table define the robot coordinate system, as reconstructed automatically based on the orientations and interfiducial distances. The actual needle trajectory is also automatically reconstructed based on the connectivity graph of all low-intensity voxels in the scan, grouped into regions of equal shortest distance from a reference (low-intensity) voxel outside the phantom. The use of these automated algorithms allows one to make optimal use of all available measurement data and also minimizes human estimation errors, resulting in subvoxel precision of reconstruction parameters.

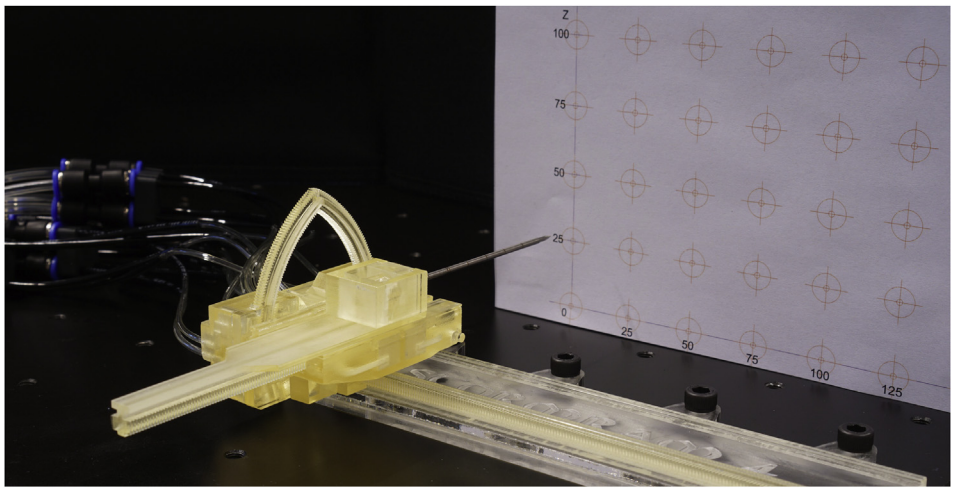

FIGURE 22.28 Stormram 4 accuracy experiment in free air.

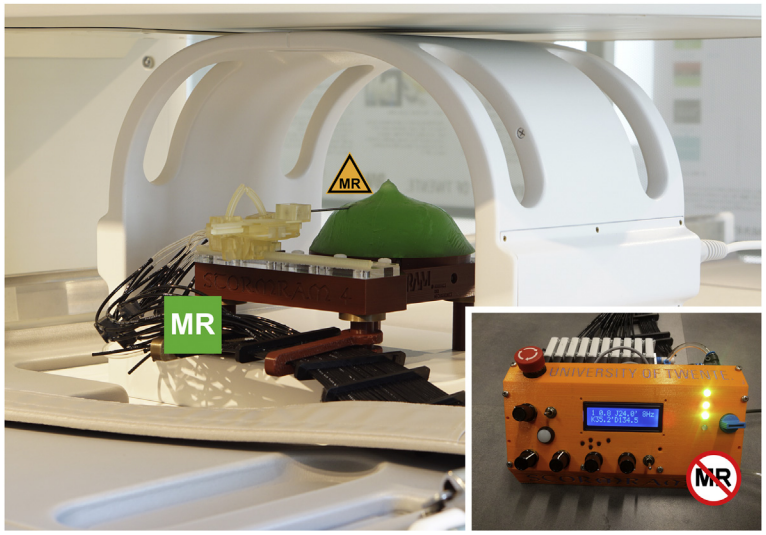

FIGURE 22.29 Measurement setup of Stormram 4 in a 0.25 T MRI scanner. *MRI*, Magnetic resonance imaging.

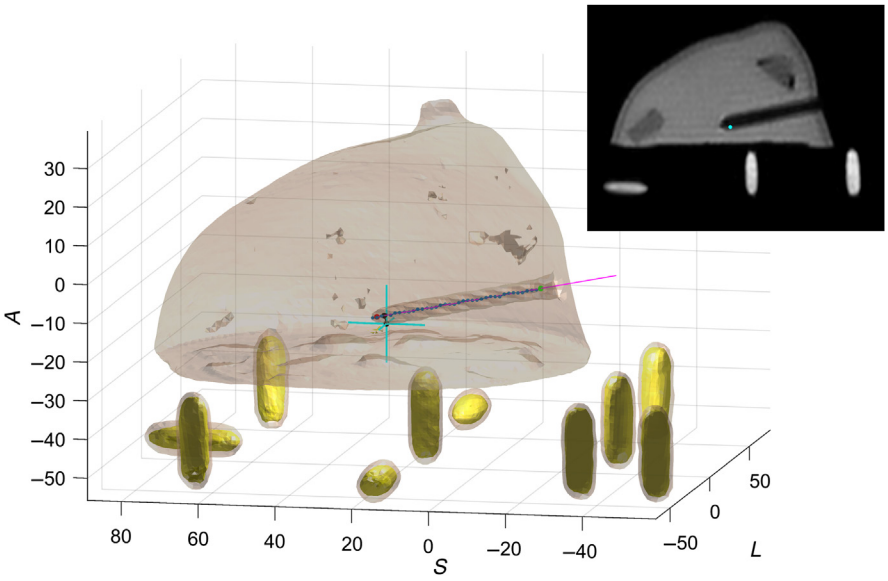

FIGURE 22.30 Three-dimensional rendering of an MRI scan consisting of a phantom with needle inserted and 10 fiducials. The crosshair indicates the target location. *MRI*, Magnetic resonance imaging.

After targeting all 30 sites, the 3D targeting error of Stormram 4 was measured to be 1.87 ± 0.80 mm (range 0.69−3.57) [24].

22.7 Conclusion

Pneumatic devices are effective in actuating MR-safe robotic systems. Several techniques for creating pneumatic actuators have been presented in this chapter: single-acting and double-acting cylinders, linear and curved stepper motors, and dual-speed stepper motor combinations.

The presented actuators offer advantages over other state-of-the-art MRI actuators in terms of compactness, output force/torque, ease of control, rapid prototypeability, and/or MR safety.

Several robotic systems have been developed for MRI-guided breast biopsy that are actuated by the described pneumatic cylinders and stepper motors. The latest generation, Sunram 5, has been shown to be a compact and versatile prototype. Thanks to the dual-speed motor implementations on two axes it combines high speed with high accuracy, especially useful in an MRI environment in which long tubes are necessary which restrict the stepping frequencies.

The pneumatic cylinders and stepper motors are manufactured by 3D printing and laser-cutting. The single-acting cylinder model is useful in exploring sealing and manufacturization techniques, while the two-cylinder stepper motor design with laser-cut teeth combines high precision with low friction and good durability.

The amount of friction depends on many factors and varies from one motor implementation to another. Measurements on several different stepper motor implementations result in efficiencies from 50% to 76%, provided that the teeth tips are sufficiently sharp, the cylinder cross-section is approximately square, and the seal dimensions are optimized to minimize friction and leakage.

The kinematic and mechanical designs of Sunram 5 are extensively described in this chapter. Based on Stormram 4's measurement results, the projected needle tip accuracy in free air is less than 1 mm, while the expected phantom targeting accuracy in MRI is in the order of 2 mm.

Given the capabilities of Sunram 5 and earlier Stormram robots, the presented pneumatic stepper motor technology has been shown to be a promising actuation technique for any MR-safe robotic system. Concerning MRI-guided breast biopsy, Sunram 5 is not yet ready for clinical use. Additional research is needed before clinical trials can be conducted, especially on calibration, path planning and control, sterilization, and safety. Sunram 5 has been shown to be an advanced proof-of-concept which may shape the future of MRI-guided robotic interventions.

References

[1] Bray F, Ferlay J, Soerjomataram I, Siegel RL, Torre LA, Jemal A. Global cancer statistics 2018: GLOBOCAN estimates of incidence and mortality worldwide for 36 cancers in 185 countries. CA Cancer J Clin 2018;68:394−424.

[2] Atchley DP, Albarracin CT, Lopez A, Valero V, Amos CI, Gonzalez-Angulo AM, et al. Clinical and pathologic characteristics of patients with BRCA-positive and BRCA-negative breast cancer. J Clin Oncol 2008;26(26):4282−8.

[3] Shellock FG, Spinazzi A. MRI safety update 2008: part 2, screening patients for MRI. AJR Am J Roentgenol 2008;191(4):1140−9.

[4] Su H, Cardona DC, Shang W, Camilo A, Cole GA, Rucker DC, et al. A MRI-guided concentric tube continuum robot with piezoelectric actuation: a feasibility study. In: 2012 IEEE international conference on robotics and automation (ICRA). IEEE; 2012. p. 1939−45.

[5] Su H, Shang W, Cole G, Li G, Harrington K, Camilo A, et al. Piezoelectrically actuated robotic system for MRI-guided prostate percutaneous therapy. IEEE/ASME Trans Mechatron 2015;20(4):1920−32.

[6] Hungr N, Bricault I, Cinquin P, Fouard C. Design and validation of a CT- and MRI-guided robot for percutaneous needle procedures. IEEE Trans Robot 2016;32(4):973−87. Available from: https://doi.org/10.1109/TRO.2016.2588884.

[7] Chapuis D, Gassert R, Ganesh G, Burdet EABE, Bleuler HABH. Investigation of a cable transmission for the actuation of MR compatible haptic interfaces. In: Biomedical robotics and biomechatronics, 2006. BioRob 2006. The first IEEE/RAS-EMBS international conference on. IEEE; 2006. p. 426−31.

[8] Yang B, Tan UX, McMillan AB, Gullapalli R, Desai JP. Design and control of a 1-DOF MRI-compatible pneumatically actuated robot with long transmission lines. IEEE/ASME Trans Mechatron 2011;16(6):1040−8. Available from: https://doi.org/10.1109/TMECH.2010.2071393.

[9] Franco E, Brujic D, Rea M, Gedroyc WM, Ristic M. Needle-guiding robot for laser ablation of liver tumors under MRI guidance. IEEE/ASME Trans Mechatron 2016;21(2):931−44. Available from: https://doi.org/10.1109/TMECH.2015.2476556.

[10] Kokes R, Lister K, Gullapalli R, Zhang B, Richard H, Desai JP. Towards a needle driver robot for radiofrequency ablation of tumors under continuous MRI. In: Robotics and automation, 2008. ICRA 2008. IEEE international conference on. IEEE; 2008. p. 2509−14.

[11] Whitney JP, Glisson MF, Brockmeyer EL, Hodgins JK. A low-friction passive fluid transmission and fluid-tendon soft actuator. In: 2014 IEEE/RSJ international conference on intelligent robots and systems. 2014. p. 2801−8. Available from: https://doi.org/10.1109/IROS.2014.6942946.

[12] Felfoul O, Becker A, Bergeles C, Dupont PE. Achieving commutation control of an MRI-powered robot actuator. IEEE Trans Robot 2015;31(2):387−99.

[13] Ho M, Kim Y, Cheng SS, Gullapalli R, Desai JP. Design, development, and evaluation of an MRI-guided SMA spring-actuated neurosurgical robot. Int J Robot Res 2015;34(8):1147–63.
[14] Stoianovici D, Kim C, Petrisor D, Jun C, Lim S, Ball MW, et al. MR safe robot, FDA clearance, safety and feasibility of prostate biopsy clinical trial. IEEE/ASME Trans Mechatron 2017;22(1):115–26. Available from: https://doi.org/10.1109/TMECH.2016.2618362.
[15] Bomers JGR, Bosboom DGH, Tigelaar GH, Sabisch J, Fütterer JJ, Yakar D. Feasibility of a 2nd generation MR-compatible manipulator for transrectal prostate biopsy guidance. Eur Radiol 2017;27(4):1776–82. Available from: https://doi.org/10.1007/s00330-016-4504-2.
[16] Stoianovici D, Patriciu A, Petrisor D, Mazilu D, Kavoussi L. A new type of motor: pneumatic step motor. IEEE/ASME Trans Mechatron 2007;12(1):98–106. Available from: https://doi.org/10.1109/TMECH.2006.886258.
[17] Bosboom DGH, Fütterer JJ, Barentsz JO. Motor system, motor, and robot arm device comprising the same, patent—WO2012069075A1. 2012.
[18] Sajima H, Kamiuchi H, Kuwana K, Dohi T, Masamune K. MR-safe pneumatic rotation stepping actuator. J Robot Mechatron 2012;24(5):820–7. Available from: https://doi.org/10.20965/jrm.2012.p0820.
[19] Sajima H, Sato I, Yamashita H, Dohi T, Masamune K. Two-DOF non-metal manipulator with pneumatic stepping actuators for needle puncturing inside open-type MRI. In: World Automation Congress (WAC), 2010. IEEE; 2010. p. 1–6.
[20] Groenhuis V, Stramigioli S. Laser-cutting pneumatics. IEEE/ASME Trans Mechatron 2016;21(3):1604–11. Available from: https://doi.org/10.1109/TMECH.2015.2508100.
[21] Abdelaziz MEMK, Groenhuis V, Veltman J, Siepel F, Stramigioli S. Controlling the Stormram 2: an MRI-compatible robotic system for breast biopsy. In: 2017 IEEE international conference on robotics and automation (ICRA). IEEE; 2017. p. 1746–53.
[22] Groenhuis V, Veltman J, Siepel FJ, Stramigioli S. Stormram 3: a magnetic resonance imaging-compatible robotic system for breast biopsy. IEEE Robot Autom Mag 2017;24(2):34–41. Available from: https://doi.org/10.1109/MRA.2017.2680541.
[23] Groenhuis V, Siepel FJ, Veltman J, Stramigioli S. Design and characterization of Stormram 4: an MRI-compatible robotic system for breast biopsy. In: 2017 IEEE/RSJ international conference on intelligent robots and systems (IROS). 2017. p. 928–33. Available from: https://doi.org/10.1109/IROS.2017.8202256.
[24] Groenhuis V, Siepel FJ, Veltman J, van Zandwijk JK, Stramigioli S. Stormram 4: an MR safe robotic system for breast biopsy. Ann Biomed Eng 2018. Available from: https://doi.org/10.1007/s10439-018-2051-5.
[25] Groenhuis V, Siepel FJ, Welleweerd MK, Veltman J, Stramigioli S. Sunram 5: an MR safe robotic system for breast biopsy. In: Hamlyn symposium on medical robotics: pioneering the next generation of medical robotics. 2018. p. 82–3.
[26] Groenhuis V, Stramigioli S. Rapid prototyping high-performance MR safe pneumatic stepper motors. IEEE/ASME Trans Mechatron 2018;23(4):1843–53.
[27] Groenhuis V, Siepel FJ, Stramigioli S. Pneumatic stepper motor and device comprising at least one such pneumatic stepper motor, patent—WO2018038608(A1). 2018.
[28] Groenhuis V, Siepel FJ, Stramigioli S, Dual-Speed MR. Safe pneumatic stepper motors. In: Robotics: science and systems 2018. 2018.
[29] Groenhuis V. Supplementary files for printing pneumatic devices. 2018. Available from: https://doi.org/10.4121/uuid:9435e52e-0d9e-4bcc-90aa-fc1a1901622c.